OPEN

NPG Asia Materials (2016) 8, e292; doi:10.1038/am.2016.97
www.nature.com/am

ORIGINAL ARTICLE

Highly anisotropic P3HT films with enhanced thermoelectric performance via organic small molecule epitaxy

Sanyin Qu[1], Qin Yao[1], Liming Wang[1], Zhenhua Chen[2], Kunqi Xu[3], Huarong Zeng[3], Wei Shi[1], Tiansong Zhang[1], Ctirad Uher[4] and Lidong Chen[1,5]

Conducting polymers are potential candidates for thermoelectric (TE) applications owing to their low thermal conductivity, non-toxicity and low cost. However, the coil conformation and random aggregation of polymer chains usually degrade electrical transport properties, thus deteriorating TE performance. In this work, we fabricated poly(3-hexylthiophene) (P3HT) films with highly oriented morphology using 1,3,5-trichlorobenzene (TCB), an organic small-molecule, as a template for polymer epitaxy under a temperature gradient crystallization process. The resulting P3HT molecules, which were confirmed to be highly anisotropic by a combination of scanning electron microscopy, atomic force microscopy, polarizing microscope, polarized Raman spectroscopy, and two-dimensional-grazing incidence X-ray diffraction (GIXRD) analysis, not only markedly reduced the conjugated defects along the polymer backbone, but also effectively increased the degree of electron delocalization. These combined phenomena produced an efficient, 1D path for carrier movement and therefore resulted in enhanced carrier mobility in the TCB-treated P3HT films. The maximum values of the electrical conductivity and Seebeck coefficient were 320 S cm^{-1} and 269 μV K^{-1}, respectively. Consequently, the maximum TE power factor and ZT value at 365 K reached 62.4 μW mK^{-2} and 0.1, respectively, in the parallel direction of the TCB-treated P3HT film. To the best of our knowledge, these are the highest values reported for pure P3HT TE materials. The method of using organic small-molecule epitaxy to generate highly anisotropic polymer films is expected to be valid for many conducting polymers.
NPG Asia Materials (2016) **8,** e292; doi:10.1038/am.2016.97; published online 22 July 2016

INTRODUCTION

Organic semiconductors, especially conducting polymers, have attracted increasing interest as potential thermoelectric (TE) materials because of their mechanical flexibility, low cost and simple manufacturing processes compared with inorganic semiconductors.[1–5] Notably, the intrinsically low thermal conductivity of organic semiconductors is favorable for attaining high TE performance. The energy conversion efficiency of a TE material is evaluated by the dimensionless figure of merit: $ZT = S^2\sigma T\kappa^{-1}$ (S, σ, κ and T are the Seebeck coefficient, electrical conductivity, thermal conductivity and absolute temperature, respectively). Although the TE properties of organic materials have been greatly improved in the past 10 years, they still lag behind those of inorganic TE materials ($ZT \sim 1$) owing, in large part, to their poor electrical transport properties such as low electrical conductivity (σ) and a low Seebeck coefficient (S). Studies of various pure conducting polymers commonly demonstrate power factors of only 10^{-5} W mK^{-2}, some 2–3 orders of magnitude less than those of state-of-the-art inorganic TE materials. Usually, inorganic materials, such as PbTe, Bi_2Te_3 and Cu_2Se, have ordered crystalline structures and better electron transport than organic materials.[6–10] In conventional conducting polymers, the inter-chain and intra-chain π–π conjugations form the carrier transport channels. The carrier transport is principally controlled by the inter-chain and intra-chain hopping processes and follows the variable range hopping model. Therefore, the configuration and arrangement of polymer chains have a key impact on carrier transport. Polymer molecules generally demonstrate irregular configurations and random arrangements, which increases the π–π conjugation defects, reduces the carrier mobility and degrades TE properties. Furthermore, the uncertainty and uncontrollability of the configuration and arrangement of the polymer chains make the study of intrinsic electric and thermal transport very challenging.

Previous studies on the TE properties of conducting polymers and their composites revealed that the use of template induction with inorganic nanoparticles (for example, carbon nanotubes, graphene,

[1]State Key Laboratory of High Performance Ceramics and Superfine Microstructure, Shanghai Institute of Ceramics, Chinese Academy of Sciences, Shanghai, China; [2]Shanghai Synchrotron Radiation Facility (SSRF), Shanghai Institute of Applied Physics, Chinese Academy of Sciences, Shanghai, China; [3]Key Laboratory of Inorganic Functional Materials and Devices, Shanghai Institute of Ceramics, Chinese Academy of Sciences, Shanghai, China; [4]Department of Physics, University of Michigan, Ann Arbor, MI, USA and [5]Shanghai Institute of Materials Genome, Shanghai, China
Correspondence: Associate Professor Q Yao or Professor L Chen, State Key Laboratory of High Performance Ceramics and Superfine Microstructure and CAS Key Laboratory of Materials for Energy Conversion, Shanghai Institute of Ceramics, Chinese Academy of Sciences, 1295 Dingxi Road, Shanghai 200050, China.
E-mail: yaoqin@mail.sic.ac.cn or cld@mail.sic.ac.cn
Received 7 February 2016; revised 21 April 2016; accepted 23 April 2016

metal nanowires) increased the degree of ordering of polymer molecular arrangements and therefore improved σ and S,[11–16] but a clear explanation for the intrinsic effect of the molecular structure on electron transport is still lacking. The electron transport in a conducting polymer composite containing an inorganic dispersion phase is complex because multiple factors may influence the transport process in diverse ways. The major factors include, but are not limited to, the distribution and structural features of the inorganic particles and the organic/inorganic interfacial structure. Therefore, the fabrication of a pure polymer having a highly regular molecular configuration and a highly ordered molecular arrangement and the subsequent investigation of the effects of the molecular arrangement on the transport properties not only would provide a simple model for studying the intrinsic electric and thermal transport mechanisms of conducting polymers but also might lead to effective approaches for improving the TE performance of polymers.

Among conducting polymers, polythiophene and its derivatives have been intensively investigated as TE materials because of their appropriate energy gap, excellent doping reversibility and wide-doping ranges. For example, the derivative poly(3,4-ethylenedioxythiophene) has reportedly reached the highest TE performance of any organic material studied.[17,18] Poly(3-hexylthiophene) (P3HT) is another promising candidate as a TE material, especially with its higher solubility in common organic solvents and highly tunable molecular structure and molecular weight compared with poly(3,4-ethylenedioxythiophene).[19–25] Interest in P3HT as a TE conversion material has increased since 2010.[26–29] However, the TE properties of pure P3HT are still unsatisfactory at present, with a power factor of $<20\ \mu W\ mK^{-2}$. The poor transport of electrons is caused by the coil conformation and random aggregation of P3HT polymer chains, which is largely due to the flexible hexyl side chains.[30–33]

Organic small-molecule epitaxy is one effective way to increase the degree of ordering of polymer chains at the molecular level by using the appropriate small-molecule crystals as the epitaxial template. Usually, if the mismatch between the lattice spacing of the host (small-molecule crystals) and the guest (polymer backbones) is <10–15%, template-induced epitaxial growth is performed relatively easily.[34] The calculated space between two thiophene rings in P3HT is 0.38 nm, whereas 1,3,5-trichlorobenzene (TCB), which is a small molecule with an orthorhombic structure, has a lattice spacing of 0.39 nm along the *c* axis.[35] The mismatch of this characteristic spacing between the two materials is only 2.6%, and thus, small-molecule epitaxy should be easily realized. In addition, the TCB molecular crystals can be oriented during growth from a melt by using unidirectional cooling (creating a temperature gradient) at ~300 K. The structural analogy in the contact plane of the two species should result in the mutual orientation of the polymer backbone onto the pre-oriented small-molecule crystals. Furthermore, TCB can be easily

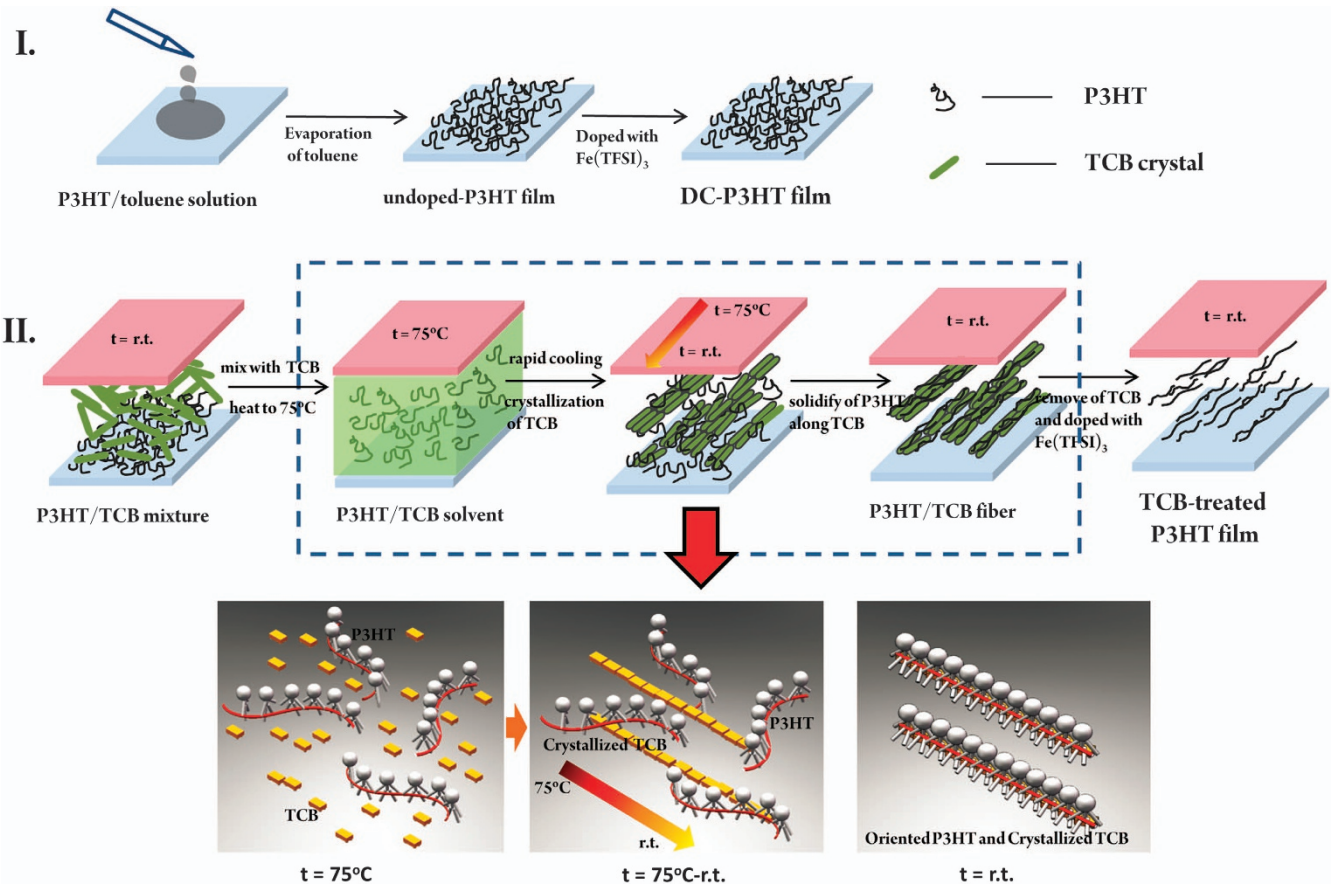

Figure 1 The schematic diagram of preparation of ordered P3HT with fiber-like texture by a two-step process. (I) The comparison P3HTfilm is prepared by drop-casting and doped by Fe $(TFSI)_3$ of nitromethane solution (DC-P3HT). (II) The undoped P3HT film is covered by small molecule 1,3,5-trichlorobenzene (TCB) powder, heated to 75 °C and then cooled rapidly from one side to the other to room temperature, forming a large temperature gradient and TCB solidified as a needle-like crystal along the temperature gradient. The P3HT polymer chains solidify on the TCB surface with polymer chains locking into the lattice of TCB due to the strong π–π conjugated interactions between the thiophene and benzene rings.

removed through vacuum evaporation or dissolution in a solvent; therefore, the construction of a pure P3HT model structure with a highly regular molecular configuration and a highly ordered molecular chain arrangement is expected.

In this paper, we report the significantly enhanced TE performance of a highly anisotropic P3HT film achieved by a temperature-gradient crystallization process using a small-molecule, TCB, as the template for polymer epitaxy. A large-scale and quasi-one-dimensional (1D) epitaxially grown P3HT film was obtained. It was found that the backbone chains of the P3HT molecules with a head-to-tail configuration (HT-P3HT) were expanded and highly oriented parallel to the fiber axis direction. The highly regular molecular configuration and highly oriented molecular arrangement of the P3HT molecules not only reduced the conjugated defects in the polymer backbone but also effectively increased the degree of electron delocalization and therefore led to enhanced carrier mobility in P3HT, which resulted in a markedly improved power factor parallel to the fiber axis.

EXPERIMENTAL PROCEDURES

Regioregular P3HT(HT-P3HT, the percentage of molecules with the head-to-tail configuration is up to 98%) ($Mw = 87\ kg\ mol^{-1}$) was purchased from Sigma-Aldrich (Shanghai, China) and used as received. TCB was purchased from TCI (Shanghai, China). Trifluoromethanesulfonimide $(CF_3SO_2)_2NH$ (95%) was purchased from Aladdin (Shanghai, China). Analytical grade nitromethane was dried over $CaCl_2$ before use.

First, regioregular P3HT powder was dissolved in toluene to make a 0.5 wt% P3HT solution and then drop-casted on a 1.8 mm × 1.8 mm clean glass substrate at 40 °C. Next, 60 mg of TCB powder was uniformly deposited onto the surface of the P3HT film and sandwiched between the P3HT-coated glass substrate and a clean glass coverslip. The 'sandwich' was then heated to the melting point of TCB (75 °C). Following heating, the 'sandwich' was slowly moved onto another bench at room temperature (25 °C). The TCB crystallized uniformly along the temperature gradient in ~1 s, and P3HT crystallized after the TCB, resulting in a color change from yellow–orange to dark violet. After removing the coverslip, the film was further doped by immersion into solution of the dopant Fetf in nitromethane ($Fe(TFSI)_3$), which was synthesized by treating freshly prepared $Fe(OH)_3$ with the acid $(CF_3SO_2)_2NH$ in anhydrous nitromethane. After doping for 1.5 h, the film was rinsed with anhydrous nitromethane and dried under vacuum at room temperature. Finally, the TCB was removed by dissolution in the nitromethane solution. The thickness of the final film was ~2 μm. The obtained product was denoted as TCB-treated P3HT (as shown in Figure 1).

For comparison, P3HT films were also fabricated by a normal drop-casting method and then doped with the Fetf nitromethane solution (using the same method as the first and third preparation steps of the TCB-treated P3HT film above), but without the TCB treatment (the second preparation step above). The product prepared with this method was denoted DC-P3HT.

The morphologies of the films were characterized by scanning electron microscopy (FEI Magellan 400 and Zeiss Supra 55) and atomic force microscopy (SPA 400, Seiko, Kobe, Japan). Polarized Raman spectra were recorded using a Dilor LabRam-1B by adjusting the holder over various angles ($\lambda = 532$ nm). Two-dimensional grazing incidence X-ray diffraction (GIXRD)

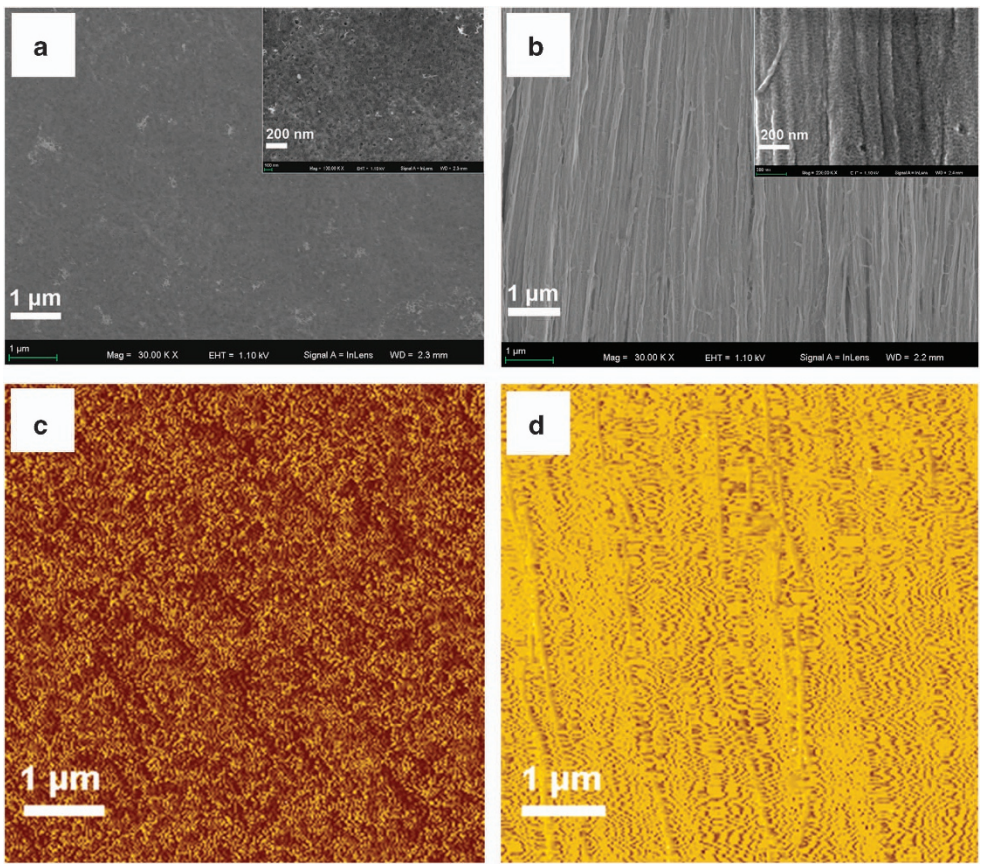

Figure 2 (**a**) SEM image of DC-P3HT film. The film displays grain structure consisting of tiny particles without any specific orientation. (**b**) SEM image of TCB-treated P3HT film. The film shows fiber structure with diameter of ~100–200 nm and closely arranged in one direction. All the fibers were composed of piles of tiny particles stacked in the direction of the fiber axis. (**c**) AFM image of phase-mode of DC-P3HT. (**d**) AFM image of phase-mode of TCB-treated P3HT. There are more crystalline regions (the bright area in the phase-mode images) in the TCB-treated P3HT film than in the DC-P3HT film.

was performed with the synchrotron X-ray source at the Shanghai Synchrotron Radiation Facility Laboratory. Optical microscopy images of the films were obtained with a XP-600 C transflective polarizing microscope with crossed polarizers. The Seebeck coefficient was measured following previously reported methods.[36] The carrier concentration and carrier mobility measurements were performed in a Quantum Design Physical Property Measurement System. The in-plane thermal conductivity was measured using the 3ω-Scanning Thermal Microscopy technique based on atomic force microscopy (SPA 400, Seiko Inc., Japan).

RESULTS AND DISCUSSION

Large-scale, highly oriented P3HT films were fabricated (Supplementary Figure S1) using TCB as the polymer epitaxial template and using a temperature-gradient crystallization process; the detailed procedure is shown in Figure 1. The scanning electron microscopy and atomic force microscopy images of the DC-P3HT film and the TCB-treated P3HT film are shown in Figure 2. In the scanning electron microscopy images, the DC-P3HT film displays a grain structure with a diameter of ~20 nm that lacks orientation (Figure 2a), whereas the TCB-treated P3HT film in Figure 2b depicts an obvious fiber structure with a diameter of ~100–200 nm that is unidirectional and closely arranged. All the fibers were composed of grains stacked in the fiber axis direction (inset of Figure 2b). The phase-mode atomic force microscopy images (Figures 2c and d) further confirm that more crystalline regions (the bright area in the images) exist in the TCB-treated P3HT films than in the DC-P3HT films.

Figure 3 displays the images of the DC-P3HT film and the TCB-treated P3HT film as observed by a polarizing microscope. The DC-P3HT film color shows no significant difference in the mutually perpendicular polarization directions (Figures 3a and b). In contrast, the TCB-treated P3HT film changes color as the polarization direction rotates; specifically, the film is nearly colorless (Figure 3c) when scanning electron microscopy the polarization direction is perpendicular to the fiber and presents a red color as the polarization direction is oriented parallel to the fiber (Figure 3d). These results reveal a birefringent nature, indicating that most of the polymer backbones are parallel to the fiber direction in the TCB-treated P3HT film.

The polarized Raman spectra of the P3HT fi7lms with two different beam directions (parallel and perpendicular to the fiber axis) give further evidence for the orientation of the polymer chains, as shown in Figure 4. The assignments of all typical Raman peaks are listed in

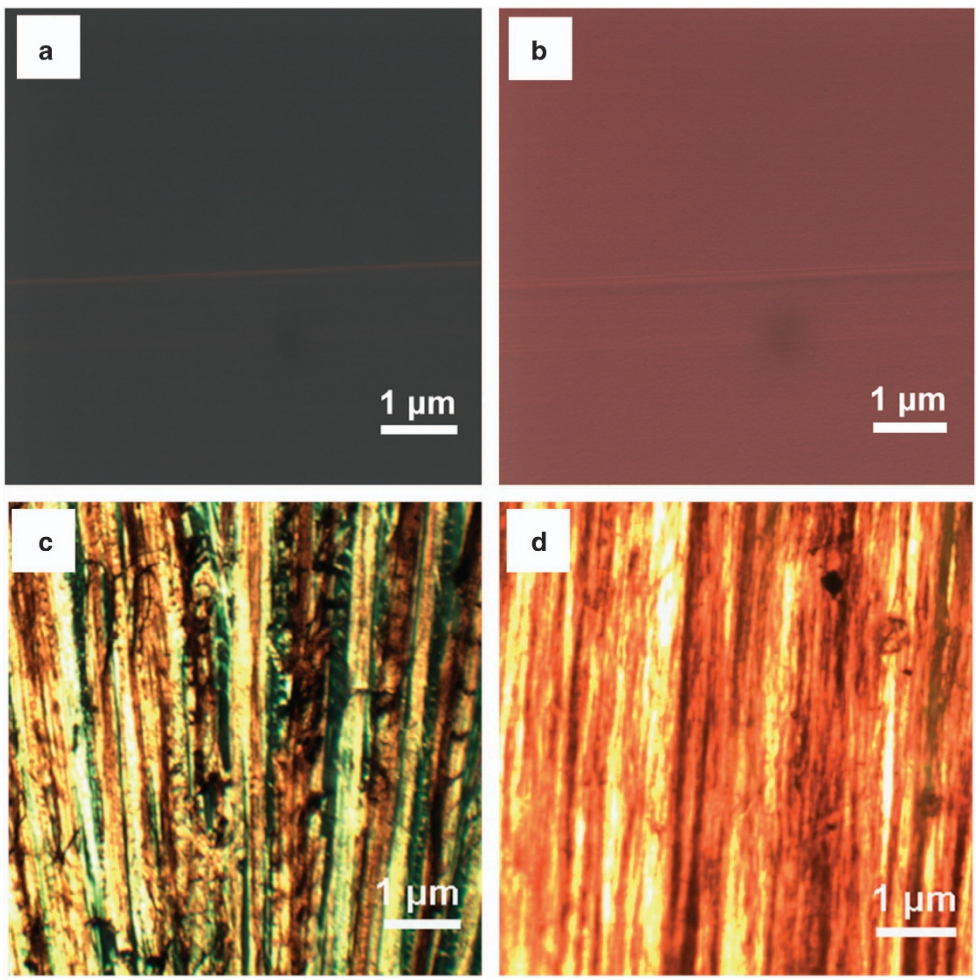

Figure 3 Images of the DC-P3HT film and the TCB-treated P3HT film are observed by a polarizing microscope. For the DC-P3HT film, the color shows no significant difference in the mutually perpendicular directions, revealing no birefringent nature of DC-P3HT (**a** and **b**). The TCB-treated P3HT film changes color upon rotation of the polarization direction. When the polarization direction is perpendicular, respectively, parallel to the fiber, the TCB-treated P3HT film shows as nearly colorless, respectively, as red (**c** and **d**). The results reveal birefringent nature of the fiber, indicating that most of the polymer backbone chains of the TCB-treated P3HT film are parallel to the fiber direction.

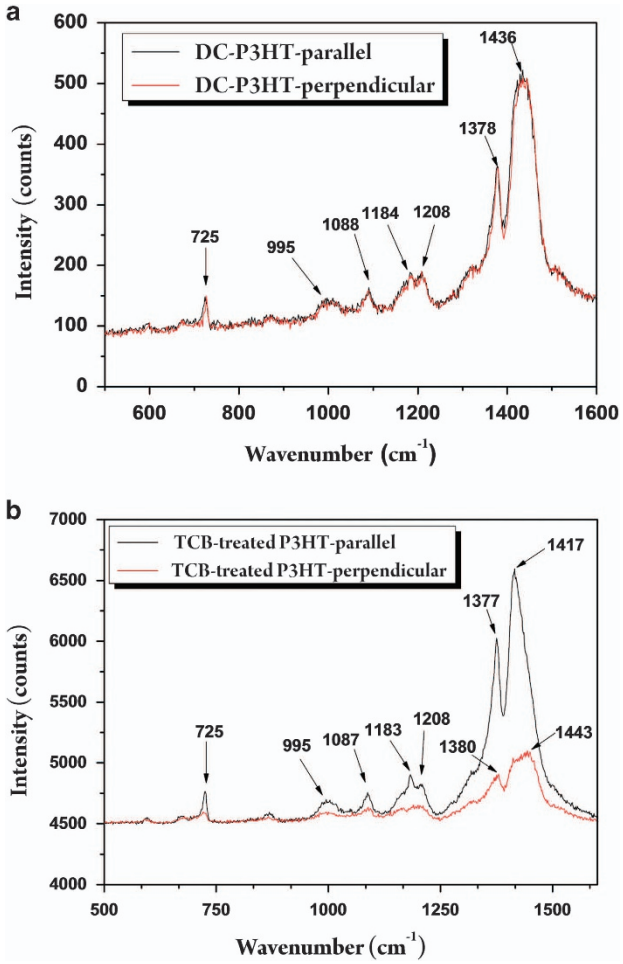

Figure 4 (**a**) Polarized Raman spectra of the DC-P3HT film under the mutually perpendicular Raman beams; the spectra of the DC-P3HT film appear almost the same in both the intensities and shifts of all the peaks in the mutually perpendicular directions. This demonstrates that the DC-P3HT film is intrinsically isotropic at a molecular scale level. (**b**) Polarized Raman spectra of the TCB-treated P3HT film under the electric field vector of the incident Raman beam perpendicular (black lines) and parallel to the fiber axis (red lines). The intensity of all the peaks is greater when the direction of the Raman beam is parallel to the fiber axis than when the direction is perpendicular to the fiber axis, further confirming that the polymer backbone chains in the TCB-treated P3HT film are aligned along the direction parallel to the fiber axis, and the number of the effective delocalized π-electrons was increased.

Table 1 The assignment of the typical Raman spectra peaks for P3HT

Raman bands (cm^{-1})	*Assignment*
~1445	Symmetric C=C stretch mode
~1381	C–C intraring stretch mode
~1208	Inter-ring C–C stretch mode
~1180	C-H bending mode with C–C inter-ring stretch mode
~1090	C–H bending
~1000	Stretching deformation between carbon and carbon of the hexyl substituent
~728	C–S–C deformation mode

Table 1. The spectra of the DC-P3HT films show almost the same intensities and shifts for all peaks under the mutually perpendicular beams (Figure 4a). This suggests that at any polarization angle, the laser beam encounters similar bonds and polarizabilities, resulting in equal absorbance intensities. These results demonstrate that the DC-P3HT film is intrinsically isotropic on the molecular scale. However, when we turn our attention to the TCB-treated P3HT film spectra, we observe that the intensities of all peaks are greater with the beam parallel to the fiber axis than in the perpendicular direction. When the majority of polymer chains are oriented in a particular direction and the incident beam is polarized in the same direction, the beam passing through the sample will encounter a larger number of C–C and C=C bonds. In addition, coupled with changes in the polarizability of the respective vibrations of C–C and C=C bonds, the agreement between polymer chain and beam orientation will result in higher absorbance intensities in that particular direction. Thus, the increase of peak intensities in the parallel direction confirms that the polymer chains in the TCB-treated P3HT film are aligned parallel to the fiber axis. Moreover, the strongest peak for the TCB-treated film in the parallel direction, occurring at ~1443 cm^{-1}, is much narrower than that for the DC-P3HT film and that in the perpendicular direction, which means a reduction in the full-width half-maximum (fwhm), indicating a higher degree of ordering in the TCB-treated film in the parallel direction. In addition, the peak corresponds to the symmetric C=C stretching mode, which is sensitive to π-electron delocalization along the backbone (conjugation length), and is shifted to the lower frequency of ~1417 cm^{-1}. Therefore, the remarkable increase in peak intensity, the narrower fwhm, and the shifting to a lower wavenumber indicate that the π–π conjugation along the backbone chain was enhanced and that the number of effectively delocalized π-electrons increased.[37,38]

To further understand the molecular chain arrangement in the DC-P3HT and TCB-treated P3HT films, 2D-GIXRD was performed at an incidence angle of 0.2° with the synchrotron X-ray source at the Shanghai Synchrotron Radiation Facility Laboratory. Figures 5a and b show the 2D-GIXRD patterns of the DC-P3HT and TCB-treated P3HT films. Figures 5c and d display the 1D diffraction profiles with respect to the out-of-plane (along the q_z) and in-plane (along the q_{xy}) directions, as extracted from the 2D-GIXRD pattern. The (h00) peak refers to the repeat distance in the direction of alkyl stacking, and (0k0) refers to the repeat distance in the direction of π–π stacking (Supplementary Figure S2). In DC-P3HT, three strong (h00) diffraction peaks and a weak (010) peak along the Debye rings were observed, indicating that the DC-P3HT film has a polycrystalline structure with mostly 'edge-on' crystallites (π–π stacking direction lying in the substrate plane) and a small amount of 'face-on' crystallites (π–π stacking direction lying out of the plane of the substrate). However, in the TCB-treated P3HT, a strong (010) π–π stacking peak coexists with the (h00) peaks along both q_z and q_{xy}. The intensity ratio of the (010) π–π stacking peak to the (h00) peak increased compared with that for the DC-P3HT, which indicates that the amount of 'face on' crystallites increased during the TCB-treated crystallization process. The increased amount of 'face-on' crystallites in TCB-treated P3HT is attributed to the mutual orientation of polymer backbones on both crystal surfaces along the *c* axis of TCB crystals during the crystallization process. Furthermore, two types of high-resolution GIXRD experiments were performed on the TCB-treated P3HT to confirm the anisotropic properties: one with the fibers parallel to the X-ray beam and the other with the fibers perpendicular to the X-ray beam, as shown in Figures 6a and b. Figures 6c and d show the 1D diffraction profiles with respect to the out-of-plane

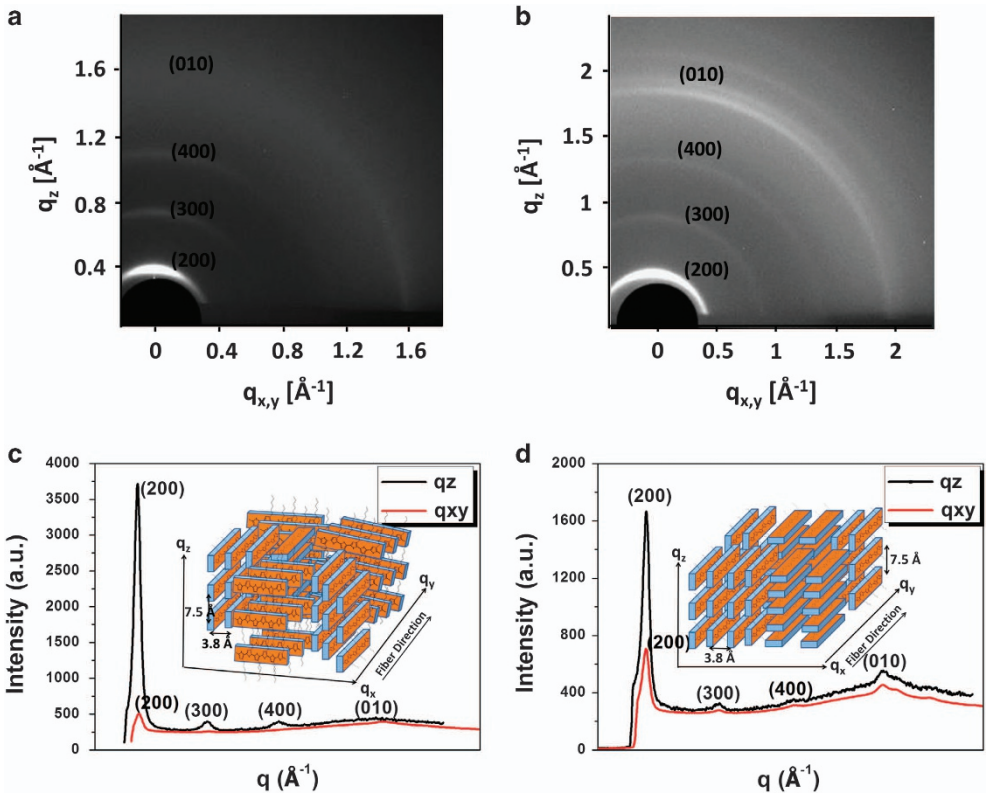

Figure 5 Two-dimensional-grazing incidence X-ray diffraction (2D-GIXRD) patterns of DC-P3HT(**a**) and TCB-treated P3HT(**b**) obtained at an incidence angle of 0.2° with the synchrotron X-ray source and (**c**), (**d**) are the 1D diffraction profile with respect to the out-of-plane (along the q_z) direction and in-plane (along the q_{xy}) direction extracted from 2D-GIXRD pattern of (**a**) and (**b**), respectively. In DC-P3HT, the observed three strong (h00) diffraction peaks and a weak (010) peak along the Debye rings indicating its polycrystalline structure with mostly 'edge-on' crystallites and a small amount of 'face-on' crystallites. In TCB-treated P3HT, there is coexistence of a strong (010) π–π stacking peak (~3.8 Å) as well as (h00) peaks along both the q_z and q_{xy}, and the intensity ratio of (010) π–π stacking peak to (h00) peak increased compared with the DC-P3HT, which indicates that the amount of 'face on' crystallites increased during the TCB-treated crystallization process. The increased amount of 'face-on' crystallites of TCB-treated P3HT is attributed to the mutual orientation of polymer backbones on both crystal surfaces along the *c* axis of TCB crystals during the crystallization process.

(along the q_z) and in-plane directions, respectively, as extracted from the 2D-GIXRD results. For the out-of-plane (q_z) profile, the specular X-ray diffraction pattern contains nearly identical Bragg diffraction peaks in both fiber directions, which correspond to d-spacings of 15.8, 11.8, 7.5 and 3.8 Å. However, for the in-plane (q_{xy}) profile, the in-plane reflection peaks are strongest when the fibers are perpendicular to the direction of the X-ray beam at d-spacings of 15.8 and 3.8 Å. Furthermore, all the in-plane reflection peaks become very weak when the axis of the fibers is parallel to the X-ray beam. The drastic drop in intensity for these peaks when probing along the fiber direction indicates that there are few repeat distances with the π–π or alkyl stacking directions along the fiber, revealing a marked anisotropy of TCB-treated P3HT. Note that the DC-P3HT film was also examined with 2D-GIXRD in two directions, but no such anisotropy was observed.

As indicated in the experimental section, the molecular configuration of the raw P3HT powder used is highly regular; namely, the percentage of head-to-tail configurations (HT-P3HT) is above 98%, which has been confirmed by NMR (shown in Supplementary Figure S3). By combining the above analyses of scanning electron microscopy, atomic force microscopy, GIXRD, polarizing microscopy and polarized Raman spectroscopy, it can be concluded that the TCB-treated P3HT molecular chains oriented along the fiber axis and that the crystallites show both 'edge on' and 'face on' patterns (inset of Figure 5d). In contrast, in the DC-P3HT film, the P3HT molecular backbones arranged randomly, with the majority in the 'edge-on' pattern (inset of Figure 5c). The high degree of orientation in the TCB-treated P3HT films, as demonstrated during characterization, proves that the strong π–π conjugation interactions and the match between the repeat distance of the thiophene units in P3HT ($C_{P3HT}/2$ ~0.38 nm) and the TCB molecules (0.39 nm) along C_{TCB} have successfully induced epitaxial growth (as shown in Figure 7). The P3HT chains locked onto the TCB lattice, forming highly ordered molecules parallel to C_{TCB} (fiber axis). Furthermore, the increased amount of 'face-on' crystallites in the TCB-treated P3HT film compared with the DC-P3HT film is additional proof of the epitaxial process, as the polymer backbones may orient on both crystal surfaces along the c-axis of TCB crystals during crystallization.

The electrical conductivity (σ) and Seebeck coefficient (S) of DC-P3HT and TCB-treated P3HT films at room temperature were measured (five samples for each fabrication condition), and the results for each condition are shown in Figure 8, with error bars. The average values for the σ and S of the DC-P3HT film are 100 S cm^{-1} and 41 μV K^{-1}, respectively, resulting in a power factor of 16 μW mK^{-2}. For the TCB-treated P3HT film, the σ in the direction parallel to the fiber axis reached 251 S cm^{-1}, which is approximately three times the value in the perpendicular direction (92 S cm^{-1}) and much higher than the conductivity of the DC-P3HT film, demonstrating obvious

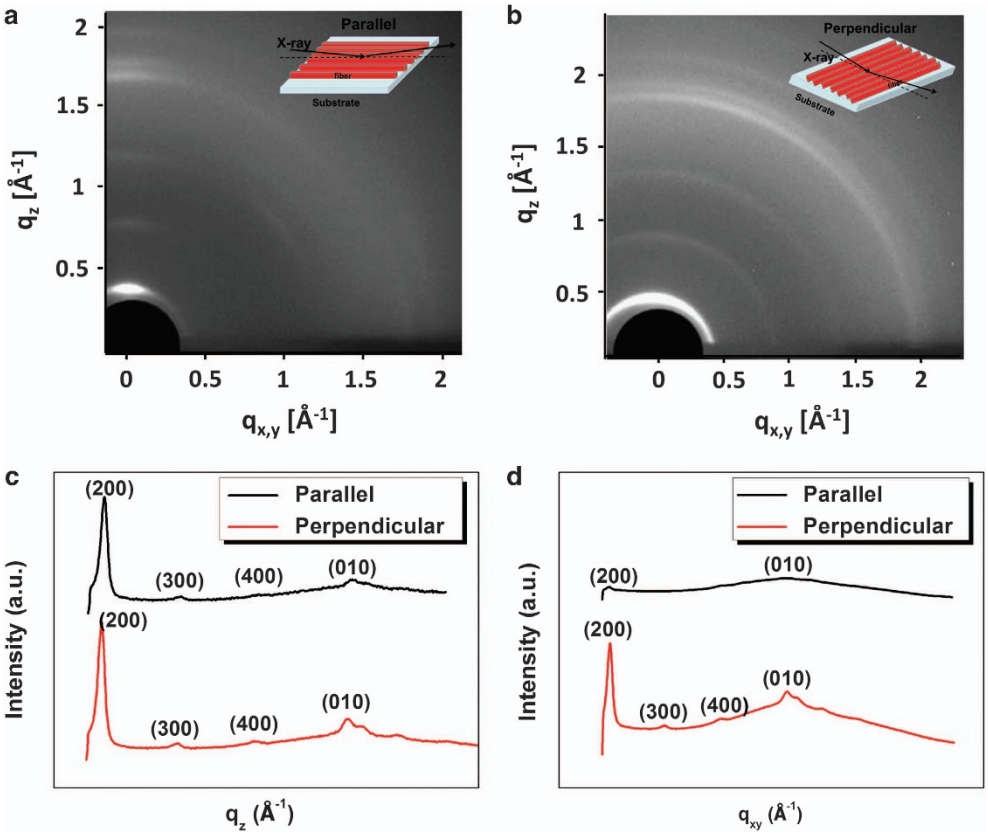

Figure 6 Two-dimensional-grazing incidence diffraction profiles of TCB-treated P3HT taken in two different orientations: (**a**) the direction of the fibers is parallel to the X-ray beam; (**b**) the direction of the fibers is vertical to the X-ray beam. (**c**) 1D diffraction profile with respect to the out-of-plane (along the q_z) direction extracted from the 2D-GIXRD results. The specular X-ray diffraction pattern contains almost the same Bragg diffraction peaks in both directions, which correspond to a d-spacing of 15.8 Å (200), 11.8 Å (300), 7.5 Å (400) and 3.8 Å (010). (**d**) 1D diffraction profile with respect to the in-plane (along the q_{xy}) direction extracted from the 2D-GIXRD results. When the fibers are vertical to the direction of the X-ray beam, the in-plane reflection peaks are much stronger at a d-spacing of 15.8 and 3.8 Å than those when the fiber axis is parallel to the X-ray beam, showing remarkable anisotropy in molecular alignment.

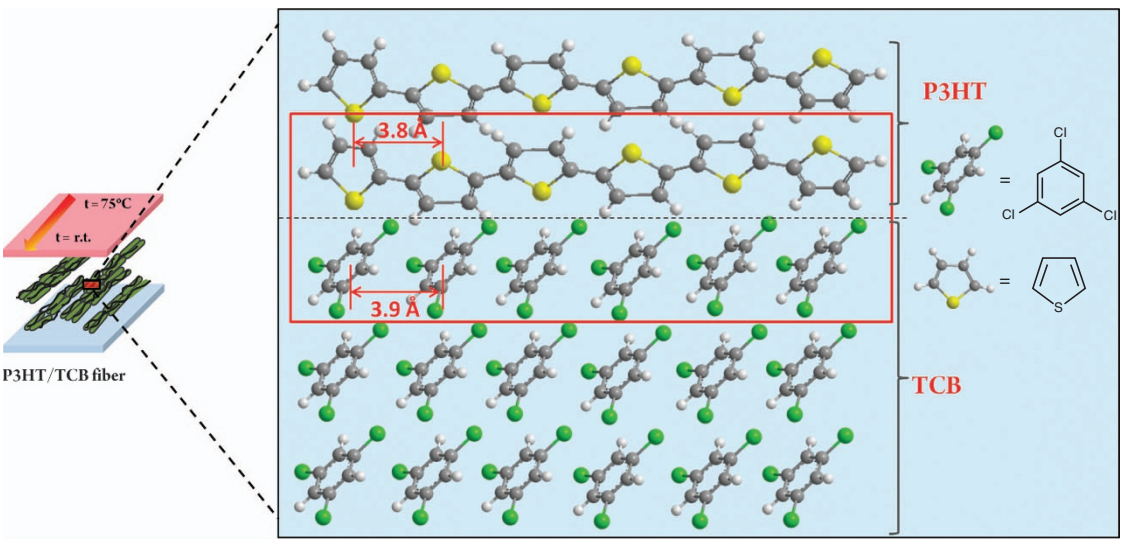

Figure 7 The characteristic high orientation of TCB-treated P3HT chains proves that the strong π–π conjugated interactions as well as the very close matching between the repeat distance of the thiophene units in P3HT ($C_{P3HT}/2$ ~0.38 nm) and the repeat distance of TCB molecules (0.39 nm) along TCB have successfully induced the epitaxy process, allowing the P3HT polymer chains to lock into the lattice of TCB, forming highly ordered P3HT chains in the direction parallel to the C_{TCB} (fiber axis).

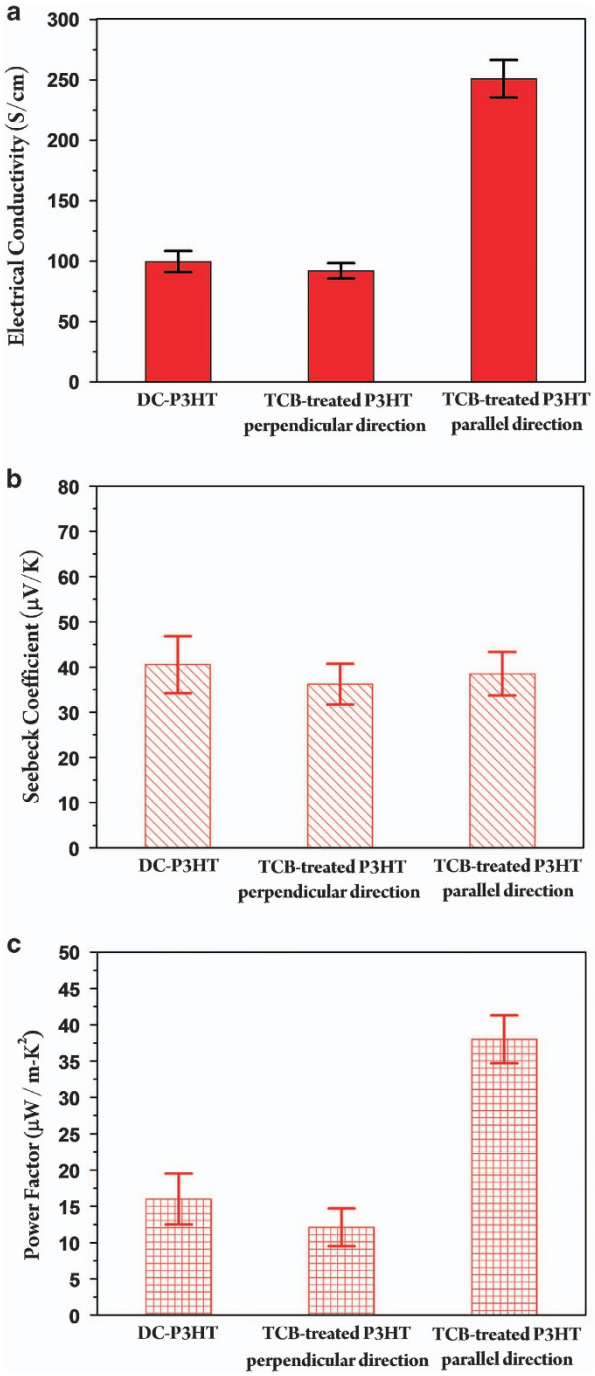

Figure 8 Electrical conductivity (**a**), Seebeck coefficient (**b**) and power factor (**c**) at room temperature of the DC-P3HT film and the TCB-treated P3HT film of five samples are shown in the error bars. The electrical conductivity of TCB-treated P3HT in the parallel direction is much higher than that in the vertical direction and that of DC-P3HT. The Seebeck coefficient do not show variable change in different directions (**b**). The power factor of the TCB-treated P3HT film in the parallel direction is up to 38 μW mK^{-2}.

anisotropy. Interestingly, the significant improvement in electrical conductivity in the parallel direction does not result in a decrease in the Seebeck coefficient, as is generally observed in a typical semiconductor. The Seebeck coefficient in the parallel direction is 39 μV K^{-1}; a similar value is obtained in the perpendicular direction and in the DC-P3HT film. As a result, the power factor (σS^2) in the parallel direction of the TCB-treated P3HT film at room temperature reached 38 μW mK^{-2}. This is not only more than three times that in the perpendicular direction of the TCB-treated P3HT film and that in the DC-P3HT film but also the highest value for a pure P3HT film ever reported, as shown in Table 2. The carrier mobility and carrier concentration of the TCB-treated P3HT and DC-P3HT films at room temperature were also measured and are listed in Table 3. The carrier mobility of the TCB-treated P3HT film is 2.5 ± 0.3 cm^2 V^{-1} s^{-1} in the direction parallel to the fiber axis, which is much higher than that in the perpendicular direction (0.9 ± 0.1 cm^{2}V^{-1} s^{-1}) and that in the DC-P3HT film (1.3 ± 0.2 cm^{2}V^{-1} s^{-1}). The carrier concentrations in the DC-P3HT film and in the TCB-treated P3HT film are similar, $\sim (4.4 \pm 0.6) \times 10^{20}$ and $(6.4 \pm 0.8) \times 10^{20}$ cm^{-3}, respectively. The enhancement in the electrical conductivity of P3HT in the parallel direction is thus mainly ascribed to an increase in carrier mobility.

Table 2 Summary of thermoelectric property of P3HT at room temperature ever reported

Matrix	*Dopant*	*Electrical conductivity (S cm^{-1})*	*Seebeck coefficient (μV K^{-1})*	*Power Factor (μW mK^{-2})*	*ZT (Evaluated)*
P3HT[1]	F_4-TCNQ	3.8×10^{-4}	400	0.006	(0.8 ~ 1.1)E-6
P3HT[2]	$NOPF_6$	2.2	25	0.14	(1.9 ~ 2.5)E-4
P3HT[3]	$FeCl_3$	7	74	3.9	(5.3 ~ 7.1)E-3
P3HT[4]	$FeCl_3$	21	30	1.9	(2.6 ~ 3.4)E-3
P3HT[5]	$NOPF_6$	10	36	1.3	(1.8 ~ 2.4)E-3
P3HT[6]	$Fe(TFSI)_3$	91	49	21.8	0.03 ~ 0.04

As the thermal conductivity of P3HT is generally ~0.15 ~ 0.2 W mK^{-1},[39-41] the evaluated ZT at room temperature is included.

The characteristic temperature dependence of the resistivity of DC-P3HT and TCB-treated P3HT films further reveals the intrinsic carrier transport properties as well as the relationship between charge transport and molecular chain arrangement, as shown in Figure 9a. It has long been recognized that conducting polymers typically contain small crystalline regions of aligned chains (ordered regions) interspersed with amorphous regions displaying randomly arranged chains (disordered regions). Moreover, Kaiser *et al.*[42] suggested that a heterogeneous model combining quasi-1D metallic conduction with hopping conduction and different dimensionality can describe the electron transport properties of conducting polymers that include both ordered and disordered regions, as follows:

$$\rho = a\rho_m \exp\left(-\frac{T_m}{T}\right) + b\rho_0 \exp\left[\left(\frac{T_0}{T}\right)^{1/n+1}\right] \quad (1)$$

Here, ρ_m, ρ_0, T_m and T_0 are the intrinsic constants (T_m is ~ 1000 K for the conducting polymer), n is the dimensionality of the hopping ($n = 1, 2, 3$) and T_0 is the characteristic Mott temperature that generally depends on carrier hopping barriers. The first contribution is related to the intrinsic quasi-1D metallic conductivity in the ordered regions, and the second term comes from the variable range hopping conduction between two ordered regions. As shown in Figure 9a, the electron transport of TCB-treated P3HT in the parallel direction fits well with the heterogeneous model combining quasi-1D metallic conduction with quasi-1D hopping conduction ($n = 1$), suggesting that the carriers pass through the disordered domains to connect ordered regions according to the quasi-1D hopping model. The charge carriers diffuse along electrically isolated disordered chains as part of

Table 3 The carrier concentration and carrier mobility of the TCB-treated P3HT film in different directions and of the DC-P3HT film

Different material	*TCB-treated P3HT-parallel*	*TCB-treated P3HT-vertical*	*DC-P3HT*
Carrier concentration (cm^{-3})	$(6.4\pm0.8)\times10^{20}$		$(4.4\pm0.6)\times10^{20}$
Electrical conductivity ($S\ cm^{-1}$)	250 ± 10	90 ± 5	95 ± 5
Carrier mobility ($cm^2\ V^{-1}\ s^{-1}$)	2.5 ± 0.3	0.9 ± 0.1	1.3 ± 0.2

Abbreviation: TCB, 1,3,5-trichlorobenzene.
The carrier mobility of TCB-treated P3HT film in the parallel direction is higher than that in the vertical direction and also higher than the mobility in DC-P3HT.

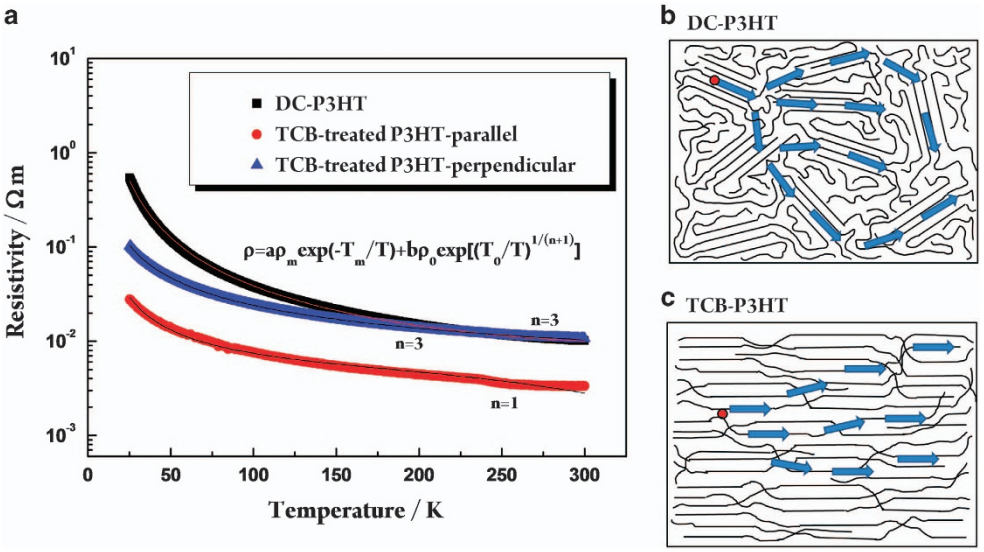

Figure 9 (**a**) The characteristic temperature dependence of the resistivity of TCB-treated P3HT and DC-P3HT films; the carrier hopping conduction between two ordered regions follows the quasi-1D hopping model (TCB-treated P3HT-parallel) and quasi-3D (DC-P3HT and TCB-treated P3HT-vertical) hopping model, respectively. (**b**) and (**c**) present schematically the path-way of the quasi-3D hopping model (**b**) and the quasi-1D model (**c**), respectively.

the conduction pathway parallel to the fiber axis as a result of the oriented 1D nature of the chains. A schematic of the process is shown in Figure 9b (the carrier hopping pathway is denoted by blue arrows). However, the temperature dependences of the resistivities of TCB-treated P3HT in the perpendicular direction and DC-P3HT films both fit the heterogeneous model, which combines quasi-1D metallic conduction with the quasi-3D hopping model. These findings suggest that when the carriers pass through disordered regions, they are delocalized and diffuse in various directions. Carriers traveling in the perpendicular direction of TCB-treated P3HT are moving between adjacent P3HT chains via 3D hopping. Owing to the existence of both 'face on' and 'edge on' patterns in TCB-treated P3HT, this 3D hopping occurs as a result of both π–π stacking and isolated side alkyl groups between adjacent P3HT chains. In DC-P3HT, the 'crystalline regions' are distributed with no particular preferred orientation, resulting in carrier hopping in any direction connecting two adjacent crystalline regions, as indicated by blue arrows in Figure 9c. This carrier hopping behavior is consistent with the morphology characterization results summarized above.

Generally, there are large quantities of inter-chain and intra-chain conjugation defects in polymers because of their irregular molecular configuration and random arrangement, which decrease carrier mobility and thus degrade the power factor.[30] In the TCB-treated P3HT film, the P3HT chains with regular molecular configurations are highly oriented parallel to the fiber axis. Moreover, the carrier hopping behavior is consistent with the morphology and proceeds via 1D hopping conduction. The highly regular molecular configuration and highly ordered molecular arrangement of P3HT not only significantly decrease the π–π conjugation defects parallel to the fiber axis but also increase the effective degree of electron delocalization, essentially producing a 1D pathway for carrier movement. As a result, the carrier mobility parallel to the fiber axis is greatly enhanced, resulting in an increased power factor.

The TE performances of DC-P3HT and TCB-treated P3HT films are further measured by changing the temperature from 300 to 500 K. Both the Seebeck coefficient and the electrical conductivity of P3HT increased as the temperature transitioned from 300 to 350 K, as shown in Figure 10. The increasing slope of TCB-treated P3HT in the parallel direction is much higher than both that in the perpendicular direction and that in the DC-P3HT film, which is probably because of the higher carrier mobility in the TCB-treated P3HT film in the parallel direction. Once the temperature passes 350 K, there are obvious variations in the electrical conductivity of the three samples, but the Seebeck coefficient continues to increase. This phenomenon may be due to a de-doping process of the conducting film, which is either caused by the chemical instability of the counterions or by a physical expulsion of counterions as a result of alkyl side chain thermal motion. Further investigation into the thermal stability should be performed, including the development of an approach to enhance the thermal stability of P3HT-based polymers. As a result, the maximum power factors of DC-P3HT and TCB-treated P3HT

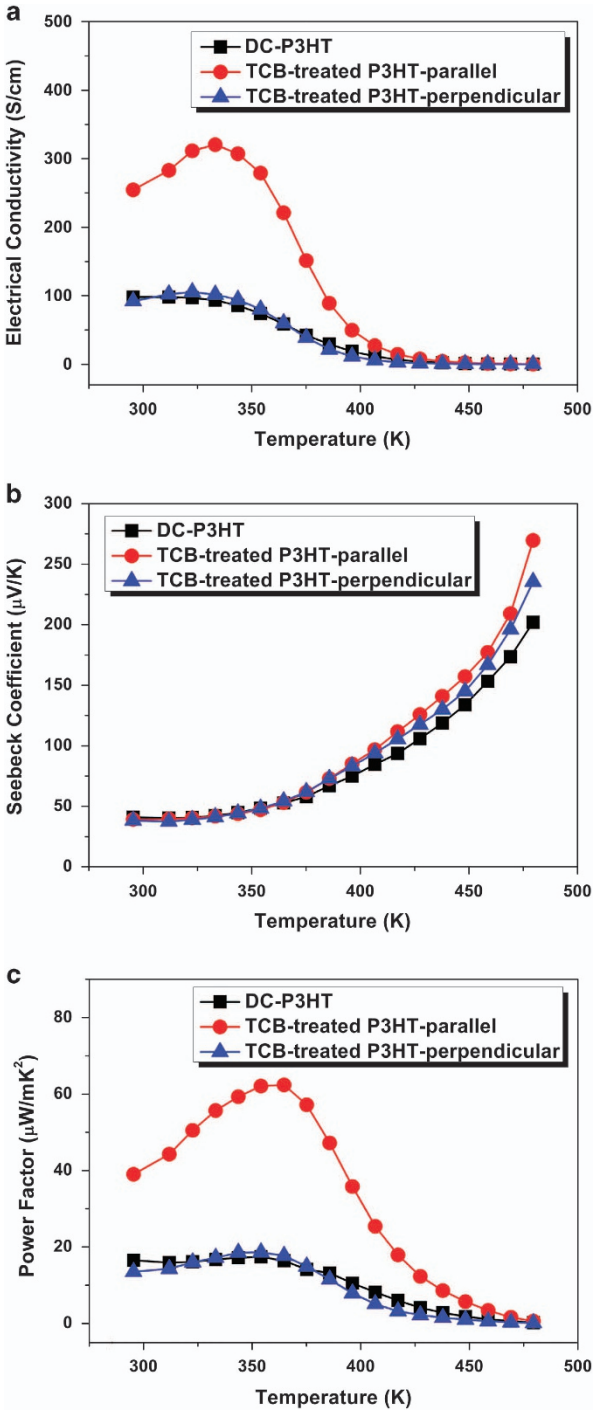

Figure 10 (**a** and **b**) Temperature dependence of the electrical conductivity and the Seebeck coefficient of the TCB-treated P3HT film in the direction parallel to the fiber axis from 295 to 480 K; (**c**) Temperature dependence of the power factor of the TCB-treated P3HT film in the direction parallel to the fiber axis from 295 to 480 K.

films in the perpendicular and parallel directions are 17.4, 18.6 and 62.4 μW mK^{-2} at 354, 354 and 365 K, respectively.

The in-plane thermal conductivity of each film was measured using the 3ω-scanning thermal microscopy technique, as shown in Supplementary Figures S4 and S5. The thermal conductivities of the films increased to ~0.16, 0.19 and 0.23 W mK^{-1} for TCB-treated P3HT in the perpendicular direction, DC-P3HT and TCB-treated P3HT in the parallel direction, respectively. However, the rate of increase in the thermal conductivity of TCB-treated P3HT in the parallel direction was not as high as expected, considering the alignment of the polymer chains. The removal of TCB molecules may leave defects between the polymer chains, which therefore act as scattering centers of phonons, suppressing the thermal conductivity. Finally, the ZT values of the P3HT films were calculated. The maximum ZT value at 365 K was estimated to be 0.10 for the TCB-treated P3HT film in the parallel direction, which is the best reported value for pure P3HT TE materials.

CONCLUSION

In summary, we fabricated large-scale, highly anisotropic P3HT films with fiber morphology via epitaxial growth on organic small-molecule TCB particles formed *in-situ* by a temperature-gradient crystallization process. During the crystallization process, rod-shaped TCB particles were first formed with a preferred orientation along the temperature-gradient direction. Next, P3HT molecules with a HT-P3HT were deposited on the TCB rods. The molecular chains oriented along the longitudinal direction of the TCB rods, forming a fiber texture. The fiber-like formations were due to strong π–π conjugated interactions as well as very close matching between the repeat distances of the thiophene units in P3HT ($C_{P3HT}/2 \sim 0.38$ nm) and the TCB molecules (0.39 nm) along C_{TCB}. After removal of the TCB by dissolution in a solvent, pure P3HT films with highly regular molecular configurations and highly ordered molecular arrangements were obtained. The ordered structure not only markedly reduced the π–π conjugated defects along the polymer backbones but also increased the effective degree of electron delocalization. Effective, 1D pathways were produced for carrier transport, and therefore, the carrier mobility of the TCB-treated P3HT film was enhanced. The maximum TE power factor and ZT value at 365 K in the parallel direction of the TCB-treated P3HT film reached 62.4 μW mK^{-2} and 0.1, respectively, the highest values reported for pure P3HT TE materials and more than three times the values measured on the film perpendicular to the fiber axis. The results presented here not only clearly demonstrate the intrinsic effects of molecular structure on the electrical transport properties of conducting polymers but also provide an effective way to enhance TE performance by manipulating the orientation of structured P3HT-based conducting polymers. Furthermore, these findings are expected to be valid for other conducting polymers.

CONFLICT OF INTEREST

The authors declare no conflict of interest.

ACKNOWLEDGEMENTS

This work was supported by the National Basic Research Program of China (973 Program) (2013CB632500), the Key Research Program of the Chinese Academy of Sciences (Grant no. KGZD-EW-T06), a research grant from the Shanghai government (Grant no.15JC1400301) and the Program of Shanghai Municipal Natural Science Foundation (Grant no. 16ZR1414100). We thank beamline 14B1 of the Shanghai Synchrotron Radiation Facility (SSRF, Shanghai, China) for the GIXRD measurement.

1 Zhang, Q., Sun, Y. M., Xu, W. & Zhu, D. B. Organic thermoelectric materials: emerging green energy materials converting heat to electricity directly and efficiently. *Adv. Mater.* **26**, 6829–6851 (2014).
2 Chen, Y. N., Zhao, Y. & Liang, Z.Q. Solution processed organic thermoelectrics: towards flexible thermoelectric modules. *Energy Environ. Sci* **8**, 401–422 (2015).

3 Shi, K., Zhang, F. J., Di, C-A., Yan, T-W., Zou, Y., Zhou, X., Zhu, D, Wang, JY & Pei, J Toward high performance n-type thermoelectric materials by rational modification of BDPPV backbones. *J. Am. Chem. Soc*. **137**, 6979–6982 (2015).
4 Wang, N., Han, L., He, H. C., Park, N-H. & Koumoto, K. A novel high-performance photovoltaic-thermoelectric hybrid device. *Energy Environ. Sci* **4**, 3676–3679 (2011).
5 Toshima, N., Oshima, K., Anno, H., Nishinaka, T., Ichikawa, S., Iwata, A. & Shiraishi, Y. Novel hybrid organic thermoelectric materials: three-component hybrid films consisting of a nanoparticle polymer complex, carbon nanotubes, and vinyl polymer. *Adv. Mater.* **27**, 2246–2251 (2015).
6 Bell, L. E. Cooling, heating, generating power, and recovering waste heat with thermoelectric systems. *Science* **321**, 1457–1461 (2008).
7 Ioffe, A. F. Infosearch Limited, London, UK, 1957.
8 Mehta, R. J., Zhang, Y. L., Karthik, C., Singh, B., Siegel, R. W., Tasciuc, T. B. & Ramanath, G. A new class of doped nanobulk high-figure-of merit thermoelectrics by scalable Bottom-up assembly. *Nat. Mater.* **11**, 233–240 (2012).
9 Tang, X. F., Xie, W. J., Li, H., Zhao, W. Y., Zhang, Q. J. & Niino, M. Preparation and thermoelectric transport properties of high-performance p-type Bi_2Te_3 with layered nanostructure. *Appl. Phys. Lett.* **90**, 012102–012102-3 (2007).
10 Liu, H. L., Shi, X., Xu, F. F., Zhang, L. L., Zhang, W. Q., Chen, L. D., Li, Q, Uher, C, Day, T & Snyder, GJ Copper ion liquid-like thermoelectrics. *Nat. Mater.* **11**, 422–425 (2012).
11 Yao, Q., Chen, L. D., Zhang, W. Q., Liufu, S. Q. & Chen, X. H. Enhanced thermoelectric performance of single-walled carbon nanotubes/polyaniline hybrid nanocomposites. *ACS Nano.* **4**, 2445–2451 (2010).
12 Meng, C. Z., Liu, C. H. & Fan, S. S. A promising approach to enhanced thermoelectric properties using carbon nanotube networks. *Adv. Mater.* **21**, 535–539 (2009).
13 King, R. C. Y., Roussel, F., Brun, J-F. & Gors, C. Carbon nanotube-polyaniline nanohybrids: influence of the carbon nanotube characteristics on the morphological, spectroscopic, electrical and thermoelectric properties. *Synth. Met* **162**, 1348–1356 (2012).
14 Bounioux, C., Diaz-Chao, P., Campoy-Quiles, M. & Muller, C. Thermoelectric composites of poly(3-hexylthiophene) and carbon nanotubes with a large power factor. *Energy Environ. Sci* **6**, 918–925 (2013).
15 Kim, D., Kim, Y., Choi, K., Grunlan, J. C. & Yu, C. Improved thermoelectric behavior of nanotube-filled polymer composites with poly(3,4-ethylenedioxythiophene) poly(styrenesulfonate). *ACS Nano.* **4**, 513–523 (2010).
16 Yu, C., Choi, K., Yin, L. & Grunlan, J. C. Light-weight flexible carbon nanotube based organic composites with large thermoelectric power factors. *ACS Nano.* **5**, 7885–7892 (2011).
17 Kim, G-H., Shao, L., Zhang, K. & Pipe, K. P. Engineered doping of organic semiconductors for enhanced thermoelectric efficiency. *Nat. Mater.* **12**, 719–723 (2013).
18 Bubnova, O., Khan, Z. U., Malti, A., Braun, S., Fahlman, M., Berggren, M. & Crispin, X. Optimization of the thermoelectric figure of merit in the conducting polymer Poly(3,4-ethylenedioxythiophene). *Nat. Mater.* **10**, 429–433 (2011).
19 Yang, X. N., Loos, J., Veenstra, S. C., Verhees, W. J. H., Wienk, M. M., Kroon, J. M., Michels, MA & Janssen, RA Nanoscale morphology of high-performance polymer solar cells. *Nano Lett.* **5**, 579–583 (2005).
20 He, Y. J., Chen, H-Y., Hou, J. H. & Li, Y. F. Indene-C(60) bisadduct: a new acceptor for high-performance polymer solar cells. *J. Am. Chem. Soc.* **132**, 1377–1382 (2010).
21 Chang, M., Lee, J., Klenhenz, N., Fu, B. Y. & Reichmanis, E. Photoinduced anisotropic supramolecular assembly and enhanced charge transport of Poly(3-hexylthiophene) thin films. *Adv. Funct. Mater.* **24**, 4457–4465 (2014).
22 DeLongchamp, D. M., Kline, R. J., Jung, Y., Germack, D. S., Lin, E. K., Moad, A. J., Richter, LJ, Toney, MF, Heeney, M & McCulloch, I. Controlling the orientation of terraced nanoscale 'Ribbons' of a Poly(thiophene) semiconductor. *ACS Nano.* **3**, 780–787 (2009).
23 Rivnay, J., Jimison, L. H., Northrup, J. E., Toney, M. F., Noriega, R., Lu, S. F., Marks, TJ, Facchetti, A & Salleo, A. A large modulation of carrier transport by grain-boundary molecular packing and microstructure in organic thin films. *Nat. Mater.* **8**, 952–958 (2009).
24 Sele, C. W., Kjellander, B. K. C., Niesen, B., Thornton, M. J., Putten, J. B. H., Myny, K., Wondergem, HJ, Moser, A, Resel, R, van Breemen, AJ, van Aerle, N, Heremans, P, Anthony, JE & Gelinck, GH Controlled deposition of highly ordered soluble acene thin films: effect of morphology and crystal orientation on transistor performance. *Adv. Mater.* **21**, 4926–4931 (2009).
25 Kline, R. J., McGehee, M. D., Kadnikova, E. N., Liu, J. & Frechet, J. M. J. Controlling the field-effect mobility of regioregular polythiophene by changing the molecular weight. *Adv. Mater.* **15**, 1519–1522 (2003).
26 Sun, J., Yeh, M. L., Jung, B. J., Zhang, B., Feser, J., Majumdar, A. & Katz, H. E. Simultaneous increase in Seebeck coefficient and conductivity in a doped Poly (alkylthiophene) blend with defined density of states. *Macromolecules* **43**, 2897–2903 (2010).
27 Xuan, Y., Liu, X., Desbief, S., Leclere, P., Fahlman, M., Lazzaroni, R., Berggren, M., Cornil, J., Emin, D. & Crispin, X. Thermoelectric properties of conducting polymers: the case of Poly(3-hexylthiophene). *Phys. Rev. B.* **82**, 115454–115463 (2010).
28 He, M., Ge, J., Lin, Z. Q., Feng, X. H., Wang, X. W., Lu, H. B., Yang, Y. L. & Qiu, F. Thermopower enhancement in conducting polymer nanocomposites via carrier energy scattering at the organic-inorganic semiconductor interface. *Energy Environ. Sci* **5**, 8351–8358 (2012).
29 Zhang, Q., Sun, Y. M., Xu, W. & Zhu, D. B. Thermoelectric energy from flexible P3HT films doped with a Ferric salt of triflimide anions. *Energy Environ. Sci* **5**, 9639–9644 (2012).
30 Kline, R. J. & Mcgehee, M. D. Morphology and charge transport in conjugated polymers. *J. Macro. Sci, Part C: Polym. Rev.* **46**, 27–45 (2006).
31 Sirringhaus, H., Brown, P. J., Friend, R. H., Nielsen, M. M., Bechgaard, K., Langeveld, B. M. W., Spiering, A. J. H., Janssen, R. A. J., Meijer, E. W., Herwig, P. T. & Leeuw, D. M. Two-dimensional charge transport in self-organized, high-mobility conjugated polymers. *Nature* **401**, 685–688 (1999).
32 Kline, R. J., Mcgehee, M. D. & Kadnikova, E. N. The dependence of regioregular Poly(3-Hexylthiophene) film morphology and Field-Effect mobility on molecular weight. *Macromolecules* **38**, 3312–3319 (2005).
33 Yao, Q., Wang, Q., Wang, L. M. & Chen, L. D. The synergic regulation of conductivity and Seebeck coefficient in pure Polyaniline by chemically changing the ordered degree of molecular chains. *Energy Environ. Sci* **7**, 2634–2640 (2014).
34 Wittmann, J. C. & Lotz, B. Epitaxial crystallization of polymers on organic and polymeric substrates. *Prog. Polym. Sci.* **15**, 909–948 (1990).
35 Belaaraj, A., Chanh, N. & Haget, Y. Crystal data for 1,3,5-trichlorobenzene and 1,3,5-tribromobenzene at 293 K. *J. Appl. Cryst.* **17**, 211 (1984).
36 Wang, Q., Yao, Q., Chang, J. & Chen, L. D. Enhanced thermoelectric properties of CNT/PANI composite nanofibers by highly orienting the arrangement of polymer chains. *J. Mater. Chem.* **22**, 17612–17618 (2012).
37 Tsoi, W. C., James, D. T., Kim, J. S., Nicholson, P. G., Murphy, C. E., Bradley, D. D. C., Nelson, J & Kim, JS The nature of in-plane skeleton raman modes of P3HT and their correlation to the degree of molecular order in P3HT:PCBM blend thin films. *J. Am. Chem. Soc.* **133**, 9834–9843 (2011).
38 Park, M. S., Aiyar, A., Park, J. O., Reichmanis, E. & Srinivasarao, M. Solvent evaporation induced liquid crystalline phase in poly(3-hexylthiophene). *J. Am.Chem. Soc.* **133**, 7244–7247 (2011).
39 He, M., Ge, J., Lin, Z., Feng, X., Wang, X., Lu, H., Yang, Y. & Qiu, F. Thermopower enhancement in conducting polymer nanocomposites via carrier energy scattering at the organic-inorganic semiconductor interface. *Energy Environ. Sci* **5**, 8351–8358 (2012).
40 Malen, J. A., Baheti, K., Tong, T., Zhao, Y., Hudgings, J. A. & Majumdar, A. Optical measurement of thermal conductivity using fiber aligned frequency domain thermoreflectance. *J. Heat Transfer* **133**, 081601–081601-7 (2011).
41 Bounioux, C., Diaz-Chao, P., Campoy-Quiles, M., Martin-Gonzalez, M. S., Goni, A. R., Yerushalmi-Rozen, R. & Muller, C. Thermoelectric composites of poly(3-hexylthiophene) and carbon nanotubes with a large power factor. *Energy Environ. Sci* **6**, 918 (2013).
42 Kaiser, A. B. Systematic conductivity behavior in conducting polymers: effects of heterogeneous disorder. *Adv. Mater.* **13**, 927–941 (2001).

Supplementary Information accompanies the paper on the NPG Asia Materials website (http://www.nature.com/am)